Scientific Reports

https://doi.org/10.1038/s41598-026-44554-w

Article in Press

A new isolated fungus *Talaromyces* sp. MC-F2 efficiently solubilizes phosphate through media-dependent metabolic regulation

Received: 6 January 2026

Accepted: 12 March 2026

Published online: 19 March 2026

Cite this article as: Xia M., Bao P., He S. *et al.* A new isolated fungus *Talaromyces* sp. MC-F2 efficiently solubilizes phosphate through media-dependent metabolic regulation. *Sci Rep* (2026). https://doi.org/10.1038/s41598-026-44554-w

Mingchen Xia, Peng Bao, Shilong He, Guanzhou Qiu, Weimin Zeng & Yu He

A new isolated fungus *Talaromyces* sp. MC-F2 efficiently solubilizes phosphate through media-dependent metabolic regulation

Mingchen Xia[a], Peng Bao[b], Shilong He[a], Guanzhou Qiu[c,d], Weimin Zeng[c,d], Yu He[a]

[a] School of Environment and Spatial Informatics, China University of Mining and Technology, Xuzhou 221116, China

[b] School of Chemical Engineering & Technology, China University of Mining and Technology, Xuzhou, 221116, China

[c] School of Minerals Processing and Bioengineering, Central South University, Changsha 410083, China

[d] Key Laboratory of Biometallurgy, Ministry of Education, Changsha 410083, China

[] Corresponding author at: School of Environment and Spatial Informatics, China University of Mining and Technology, Xuzhou 221116, China

Email addresses: mingchen2011@yeah.net (M. Xia). ORCID: 0000-0001-5259-2640

Abstract: This study isolated and identified a new phosphate-solubilizing fungus strain, *Talaromyces* sp. MC-F2, based on morphological characteristics and phylogenetic analysis, from agricultural soil. Its capacity to solubilize tricalcium phosphate (TCP) was systematically evaluated in Pikovskaya (PVK), National Botanical Research Institute's phosphate growth medium (NBRIP), and potato dextrose broth (PDB) media. MC-F2 demonstrated effective TCP dissolution across all media, and the highest final concentration of soluble phosphorus was observed in NBRIP medium. The solubilization was primarily driven by acidification through secretion of organic acids, notably gluconic and malic acid, leading to the formation of calcium oxalate hydrates (whewellite and weddellite) as secondary minerals. Untargeted metabolomics revealed that medium composition and TCP concentration significantly reshaped central metabolic pathways, particularly enhancing the TCA cycle in NBRIP, which directly underpinned the high organic acid production and superior solubilization performance. These findings not only expand the resources of phosphate-solubilizing fungi but also provide deeper metabolic insights into their environmental adaptability, highlighting the potential of *Talaromyces* sp. MC-F2 as a promising agent for developing eco-friendly biofertilizers.

Keywords: Phosphate-solubilizing fungus; *Talaromyces*; Tricalcium phosphate; Culture media; untargeted metabolomics

Introduction

Phosphorus (P) is an essential macronutrient for the growth and development of plants [1,2]. However, the majority of P is present in insoluble forms (e.g., Ca-P, Al-P, Fe-P) in agricultural soils, with only a minute fraction (≈0.1%) directly available for plant uptake [3,4]. While chemical P fertilizers are routinely applied to overcome this limitation, their excessive use leads to environmental issues such as soil acidification, eutrophication, and loss of soil microbial diversity [5,6]. Consequently, there is an urgent need to develop sustainable strategies to enhance P availability.

Phosphate-solubilizing microorganisms (PSMs), including bacteria (PSB), fungi (PSF), and actinomycetes (PSA), convert insoluble P into plant-available forms and represent efficient and eco-friendly biofertilizers [7]. Among these, PSF are often considered more effective due to their extensive hyphal networks, which increase the mineral contact area, and their generally higher production of organic acids [8,9].

The phosphate-solubilizing activity of PSF is primarily mediated through acidification (via organic acid secretion) and enzymatic hydrolysis (via phosphatases) [4]. However, the metabolic regulation of these processes in response to environmental factors, such as medium composition and P source concentration, remains inadequately understood. Metabolomics offers a powerful tool to detect low molecular weight metabolites and discover the metabolic differences under different environmental conditions [10].

Although classical media such as Pikovskaya (PVK) [11] and the National Botanical Research Institute's phosphate growth medium (NBRIP) [12] are standard for evaluating P solubilization, and potato dextrose broth (PDB) is commonly used for fungal cultivation [13], systematic comparisons of PSF performance across these media are scarce. Furthermore, research has predominantly focused on *Aspergillus* and *Penicillium* species [9,14], leaving the potential of other fungal genera, such as *Talaromyces*, largely unexplored.

Therefore, this study aimed to (1) isolate and identify a novel PSF strain; (2) systematically evaluate its phosphate-solubilizing capacity in PVK, NBRIP, and PDB media with varying tricalcium phosphate (TCP) concentrations; (3) characterize the secondary minerals formed and the organic acids produced; and (4) employ untargeted metabolomics to elucidate the metabolic pathways influenced by medium type and TCP concentration. This work expands the repository of PSF resources and provides deeper metabolic insights into fungal phosphate solubilization.

Methods

Culture media

Three types of media were used for PSF cultivation. PVK liquid medium is composed of 10 g/L of glucose, 5.0 g/L of TCP, 0.5 g/L of $(NH_4)_2SO_4$, 0.3 g/L of $MgSO_4 \cdot 7H_2O$, 0.3 g/L of NaCl, 0.3 g/L of KCl, 0.5 g/L of yeast extract, 0.03 g/L of $MnSO_4 \cdot 4H_2O$ and 0.03 g/L of $FeSO_4 \cdot 7H_2O$ [11]. NBRIP liquid medium is composed of 10 g/L of glucose, 5.0 g/L of TCP, 0.1 g/L of $(NH_4)_2SO_4$, 5 g/L of $MgCl_2 \cdot 6H_2O$,

0.25 g/L of $MgSO_4 \cdot 7H_2O$ and 0.2 g/L of KCl [12]. PDB contains 6g/L of potato extract and 20g/L of glucose. 15g/L of agar was added to solidify media and named as PVKA, NBRIPA and PDA medium, respectively. All above chemical reagents are analytical grade. All media were autoclaved at 121℃ for 20min before inoculation.

Isolation and identification of a PSF strain

Soil samples were collected from agricultural land around a coal mining subsidence area in Anhui Province, China. Permission has been obtained from the landowner for sample collection. The soil physiochemical properties were analyzed and shown in Table S1. 5g of raw soil samples were added to 150mL Erlenmeyer flasks with 50mL of sterile normal saline. After shaking for 24h in a rotary shaker at 25℃, 160rpm, 1mL of soil suspension was sampled and diluted to 10^{-1} ~ 10^{-9}. 0.5mL of each dilution was added to PVKA plates and dispersed uniformly using coating method. All plates were cultured for 7 days at 30℃ in a constant temperature incubator. Multiple colonies exhibiting clear transparent halos were observed. The strain forming the largest and most distinct halo (halo-to-colony diameter ratio > 2.0) was selected, designated MC-F2, and purified through repeated streaking on fresh PVKA plates.

The individual fungal colony was inoculated into PDB medium and cultivated for 2~3 days in a rotary shaker at 30℃, 160rpm. Genomic DNA was extracted from hyphae using Fungal Genomic DNA Kit (Solarbio, Beijing) following manufacturer's instructions. The internal transcribed spacer (ITS) was amplified with the primers ITS1 (5'-TCCGTAGGTGAACCTGCGG-3') and ITS4 (5'-

TCCTCCGCTTATTGATATGC-3’). To enhance taxonomic resolution, the β-tubulin (BenA) gene was also amplified and sequenced using primers Bt2a (5'-GGTAACCAAATCGGTGCTGCTTTC-3') and Bt2b (5'-ACCCTCAGTGTAGTGACCCTTGGC-3') [15]. ITS and β-tubulin sequences were determined by Sangon Biotech Co., Ltd (Shanghai, China) and analyzed on NCBI GenBank using BLAST program. MEGA11 software was used for phylogenetic analysis based on neighbor-joining method with Jukes-Cantor model. No. of bootstrap replications was 1000. Phylogenetic trees were constructed using both ITS and β-tubulin sequences.

Phosphate-solubilizing capacity test

After activation on PDA medium for 7 days, fresh conidia of the isolated PSF strain were obtained and diluted with sterile normal saline as a spore suspension (10^7 CFU/mL). 1mL prepared spore suspension was inoculated to 100 mL of PVK, NBRIP and PDB media in 250mL Erlenmeyer flasks, respectively. The concentration of TCP was set as 1, 2, 3, 4 and 5g/L. In particular, PVK, NBRIP and PDB media containing 1g/L or 5g/L TCP were labeled as PVK1, PVK5, NBRIP1, NBRIP5, PDB1 and PDB5, respectively. PDB medium without TCP was labeled as PDB. No inoculation served as the abiotic control. All treatments were carried in triplicate.

Untargeted metabolomics

2mL samples from the PDB, PDB1, PDB5, PVK1, PVK5, NBRIP1 and NBRIP5 cultures were centrifuged at 5000 × g for 5 minutes at 4℃ to remove cell debris.

The obtained supernatants were then flash-quenched in liquid nitrogen for 30s, and stored at -80℃ pending untargeted metabolomics analysis.

LC-MS/MS analyses were performed using an UHPLC system (Vanquish, Thermo Fisher Scientific) with a Waters ACQUITY UPLC BEH Amide column (2.1 mm × 50 mm, 1.7μm) coupled to Orbitrap Exploris 120 mass spectrometer (Orbitrap MS, Thermo). The column temperature was kept as 25℃. The mobile phase consisted of 25 mmol/L ammonium acetate and 25 mmol/L ammonia hydroxide in water（pH = 9.75）(A) and acetonitrile (B). The linear gradient was set as follow: 0-0.25 min: 95% B, 0.25-3.5 min: 95% B to 65% B, 3.5 min to 4 min: 65% B to 40% B, 4 min to 4.5 min: 40% B, 4.5 min to 4.55 min: 40% to 95% B, 4.55 min to 6 min: 95% B. The auto-sampler temperature was 4℃. The flow rate was 0.5 mL/min and the sample injection volume was 2μL. The Orbitrap Exploris 120 mass spectrometer was used for its ability to acquire MS/MS spectra on information-dependent acquisition (IDA) mode in the control of the acquisition software (Xcalibur, Thermo). In this mode, the acquisition software continuously evaluates the full scan MS spectrum. The ESI source conditions were set as following: sheath gas flow rate as 50 Arb, Aux gas flow rate as 15 Arb, capillary temperature 320 ℃, full MS resolution as 60000, MS/MS resolution as 15000, collision energy: SNCE 20/30/40, spray voltage as 3.8 kV (positive) or -3.4 kV (negative), respectively.

Principle component analysis (PCA) was carried out to visualize the distribution and the grouping of the samples. Supervised orthogonal projections to latent structures discriminate analysis (OPLS-DA) was conducted to visualize group

separation and find significantly changed metabolites. Furthermore, the value of variable importance in the projection (VIP) of the first principal component in OPLS-DA analysis was obtained. The metabolites with VIP>1 and p<0.05 (student t test) were considered as significantly changed metabolites. In addition, commercial databases including Kyoto Encyclopedia of Genes and Genomes (KEGG) database (http://www.genome.jp/kegg/) [16] was used for pathway enrichment analysis. Three-parallel experiments were performed for metabolomic data collection and processing.

Chemical analysis

Samples from different liquid media were passed through the 0.22μm PTFE membrane filter to determine the concentrations of soluble P and organic acid, and phosphatase activities. The concentration of soluble P was measured through ammonium vanadomolybdate colorimetry [17]. Organic acids were detected by high-performance liquid chromatography (HPLC, Waters e2695) equipped with a variable UV detector and AQ-C18 column (4.6mm×250mm, 5μm). The mobile phase was 0.1% (v/v) phosphoric acid/ acetonitrile (90:10, v/v) for gluconic acid elution, and 0.01mol/L diammonium hydrogen phosphate for malic acid, citric acid, oxalic acid and tartaric acid elution. They were injected at a flow rate of 1mL/min and detected at 210nm. The sample injection volume was 20μL. Acid phosphatase (ACP) and alkaline phosphatase (AKP) activities were measured by commercial kits purchased from Nanjing Jiancheng Bioengineering Institute according to the instruction of manufacturer.

Characterization

SEM (TESCAN G0AIA3 XMH, Czech Republic) equipped with EDS (Aztec 4.1, Oxford Instruments Inc.) was used to characterize the micromorphology and element composition. The crystallization products after TCP dissolution were detected by XRD (D8 ADVANCE, Germany) with a scan range of 4-70° after filtration, drying and grinding. The composition of functional groups was analyzed by FTIR (VERTEX80V, Germany). The dried sample was mixed with KBr (1:100, w/w), and then FTIR was conducted at a resolution of 2cm^{-1}, between 4000 and 400cm^{-1}.

Statistic analysis

Data were expressed as the arithmetic mean and standard deviation. Statistical significance was determined by one-way analysis of variance (ANOVA) followed by Tukey's post hoc test using software SPSS (version 27). Pearson correlation analysis was performed to assess the relationship between pH and soluble P concentration. A significance threshold of $p < 0.05$ was applied. Figures were generated using Origin (version 9.0).

Results

Identification of the isolated PSF strain MC-F2

As displayed in Fig. S1, the colony of MC-F2 on PVKA plate initially exhibited yellow, and transformed to green over time. In contrast, the colony on PDA plate displayed a yellowish-white periphery and a pink center at early stages, later developing a uniform golden-yellow coloration. Reverse-side observation revealed

significantly greater production of pigment on PDA plate. Transparent halo appeared around the colony on three kinds of agar-solidified media (Fig. 1A). The halo-to-colony diameter ratio reached 2.22±0.15 (PVKA), 2.19±0.1 (NBRIPA) and 2.21±0.11 (PDA), respectively. It was in accord with the criteria of PSMs [18]. Furthermore, typical conidiophore of *Talaromyces* genus was observed through SEM image, and conidiospore was ovate with smooth to slightly rough wall (Fig. 1B). ITS sequence (585 bp) of MC-F2 was registered in GenBank and obtained the accession number of PQ270042. Phylogenetic relationships displayed that MC-F2 clustered with *Talaromyces* species in both ITS (Fig. 1C) and β-tubulin (Fig. S2) based trees, and shared over 97% similarity with them. Due to its low bootstrap value relative to *T. adpressus*, *T. pinophilus*, *T. sayulitensis*, and *T. verruculosus*, the isolate provisionally designated as *Talaromyces* sp. MC-F2.

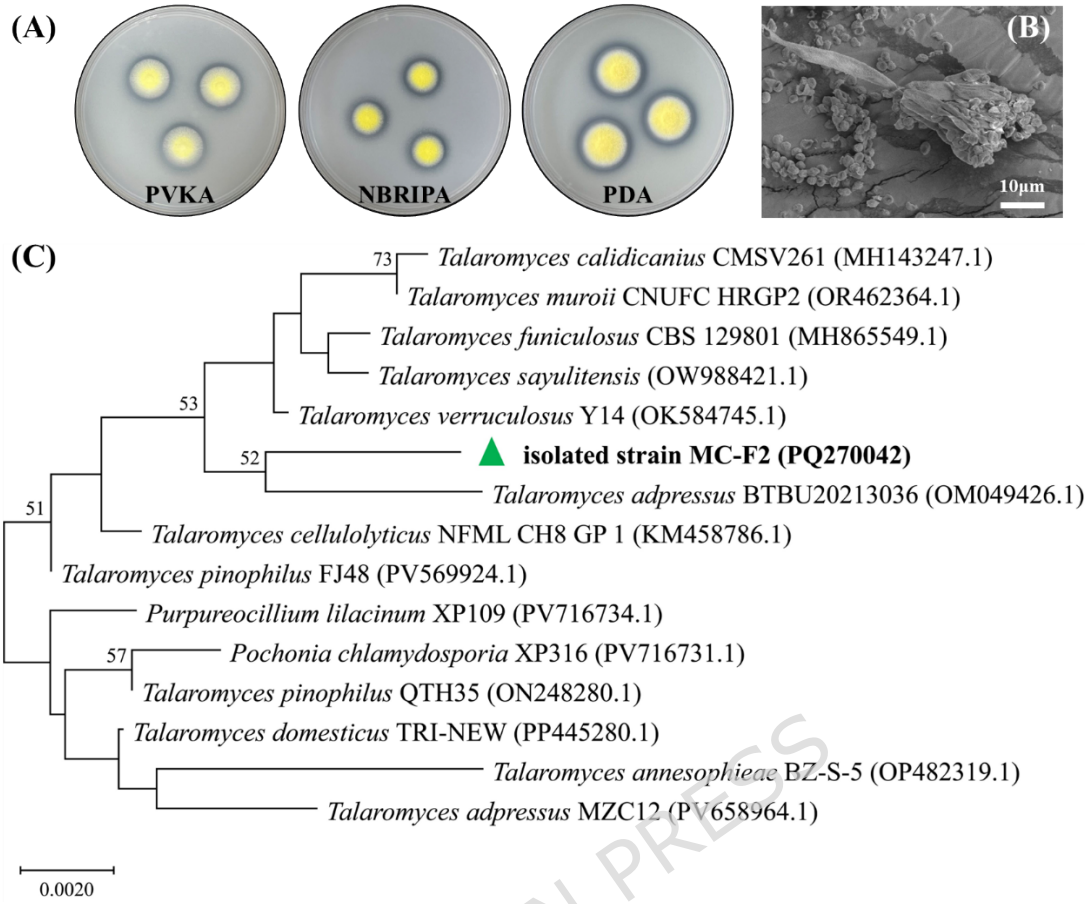

Fig. 1 Transparent halo observation (A), SEM image (B) and phylogenetic tree based on ITS gene sequence (C) of the isolated PSF strain

Evaluation of phosphate-solubilizing capacity of *Talaromyces sp.* MC-F2

Sometimes identified PSMs do not show clear transparent halo on agar-solidified plates, while they can solubilize insoluble phosphate in liquid medium [19]. So, the phosphate- solubilizing capacity of MC-F2 was further evaluated in liquid medium. As shown in Fig. 2, no obvious change of pH and a trace of soluble P were detected in abiotic control groups across PVK, NBRIP and PDA media. While MC-F2 significantly promoted TCP solubilization in all treatments, confirming that the observed solubilization was primarily biologically driven.

In detail, on day 1 in PVK medium, pH decreased to 4.00±0.14 (1g/L TCP),

4.49±0.03 (2g/L TCP), 5.02±0.06 (3g/L TCP), 5.24±0.2 (4g/L TCP) and 5.35±0.38 (5g/L TCP), respectively, with corresponding soluble P concentration reaching 358±13.83, 378±28.36, 208±33.01, 168±23.53 and 156.89±18.48mg/L. Subsequently, soluble P kept stable in 1 g/L TCP. While systems containing 2–5 g/L TCP displayed an evident increase in soluble P on day 2, followed by a slow rise until stabilization occurred between days 6–7. The peak soluble P concentration was 796.67±3.33 (2g/L TCP), 1086.35±42.84 (3g/L TCP), 1183.33±4.35 (4g/L TCP), and 1340.56±31.63 mg/L (5g/L TCP), respectively.

In NBRIP medium, only minimal soluble P was detected across all TCP concentrations on day 1, contrasting markedly with the phenomena observed in PVK medium. However, tremendous pH decrease appeared on day 2 and subsequently tended to be stable. Soluble P concentration also increased sharply on day 2 and kept rising until day 4, followed by a moderate decline. The maximum soluble P concentration reached 530±35.15 (1g/L TCP), 905±23.52 (2g/L TCP), 1255±24.02 (3g/L TCP), 1446.67±35.31 (4g/L TCP), and 1521.67±46.68 mg/L (5g/L TCP), which was consistently higher than those recorded in the PVK medium at the same TCP level.

In PDB medium, across TCP concentrations of 0–5 g/L, the pH decreased below 4.6 on day 1 and reached the minimum value on day 2 at 3.05±0.34 (0g/L TCP), 3.48±0.04 (1g/L TCP), 3.67±0.03 (2g/L TCP), 3.88±0.01 (3g/L TCP), 4.09±0.04 (4g/L TCP), and 4.22±0.02 (5g/L TCP), respectively, and then exhibited continuous pH increase. Soluble P levels on day 1 across all TCP concentrations were the

highest comparing to those in PVK and NBRIP media. The maximum soluble P concentration was 385.33±4.88 mg/L (1g/L TCP) on day 1, 605.33±4.55 (2g/L TCP), 968.67±18.27 (3g/L TCP) and 1272±4.58mg/L (4g/L TCP) on day 2, and 1518.67±42.53mg/L (5g/L TCP) on day 5, respectively.

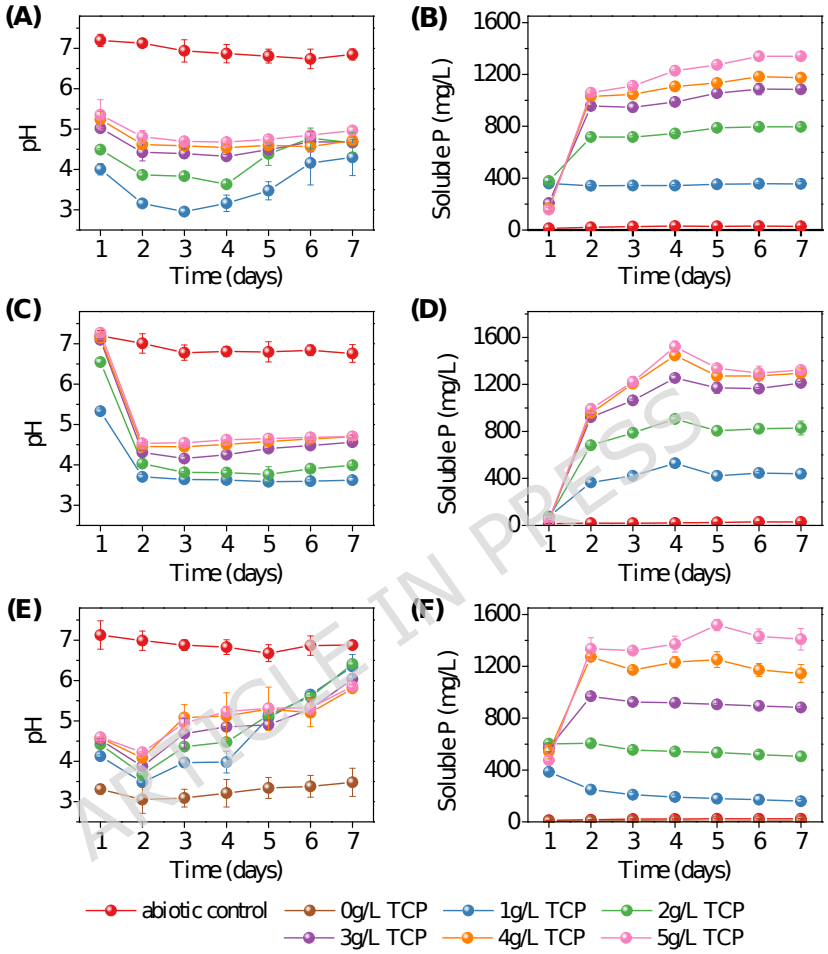

Fig. 2 Changes of pH and soluble P concentration along incubation time in PVK medium (A-B), NBRIP medium (C-D) and PDB (E-F) medium.

Statistical analysis shows that there are significant differences in the maximum soluble P concentration under different TCP concentrations in PVK, NBRIP and PDB medium, respectively (Fig. S3A). In 2–4 g/L TCP, significant differences exist among PVK, NBRIP and PDB media. While no significant difference appeared between PVK and PDB media in 1 g/L of TCP, as well as NBRIP and PDB media in

5 g/L of TCP (Fig. S3B). It should be noted that comparisons of soluble P concentration across media are based on solution measurements and are not normalized to fungal biomass.

Pearson correlation analysis between pH and soluble P concentration was shown in Fig. S4. A strong negative correlation was observed in NBRIP medium, which robustly confirms that overall acidification of the solution serves as the dominant and consistent mechanism driving phosphate dissolution in this medium. A significant negative correlation was lost only at the highest TCP concentration of 5 g/L in PDB medium. While the situation is particularly distinctive in PVK medium. A significant negative correlation was observed only at the TCP concentration of 4 g/L, while it was not significant at other concentrations.

Organic acids production and phosphatase activity detection

As shown in Fig. 3, MC-F2 produced high concentration of gluconic acid and malic acid in the tested media. Higher gluconic acid secretion by MC-F2 was associated with lower TCP concentration, while more malic acid production was observed at elevated TCP levels. The maximum yields of gluconic acid and malic acid were 1819.52±28.62mg/L in PDB medium without TCP and 6013.30±77.73mg/L in PDB medium with 5g/L TCP, respectively. Citric acid was mainly detected in PDB medium, and reached 250.43±11.03mg/L in PDB medium without TCP, 220.68±10.07 mg/L in PDB medium with 1g/L TCP, and 224.8±15.99mg/L in PDB medium with 5g/L TCP.

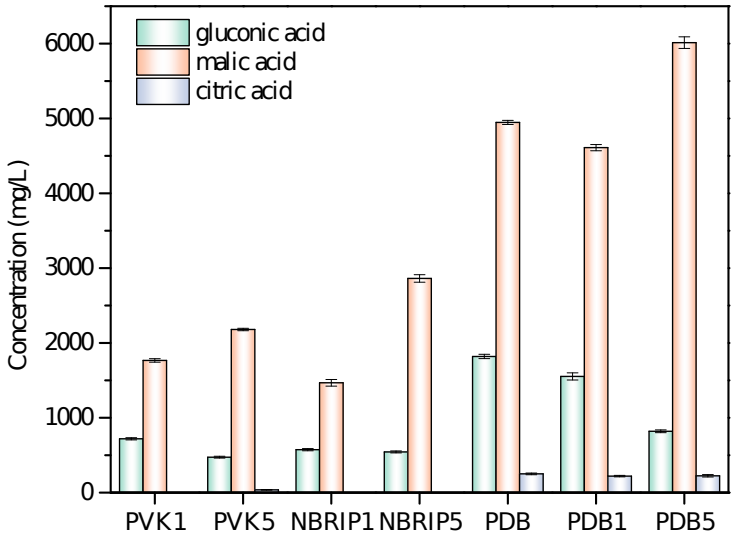

Fig. 3 Types and quantities of produced organic acids by MC-F2 in PVK, NBRIP and PDB liquid medium with 1g/L or 5g/L TCP. Data are shown as final supernatant concentration (mean ± SD, n=3).

Fig. 4 displays ACP and AKP activities in different conditions. In PVK medium, ACP activities at all TCP concentrations increased continuously during the first 5 days. By day 7, ACP activities decreased significantly in 2-5 g/L TCP, but continued to rise in 1g/L TCP. In NBRIP medium, ACP activities across all TCP concentrations remained at relatively high levels for the initial 3 days but showed a significant decline by day 5. This phenomenon was similar to that observed in PDB medium. Notably, in PDB medium without TCP, ACP activity significantly elevated, reaching its maximum on day 3. This peak activity was approximately 4.9-fold higher than those detected in groups supplemented with TCP. Therefore, it is speculated that the addition of TCP to PDB medium inhibited, to some extent, ACP synthesis by MC-F2.

Regarding AKP activity, it was low in both NBRIP and PVK media on day 1, but relatively higher in PDB medium. On day 2, AKP activity increased to varying

degrees across all media and TCP concentrations, although it showed no significant correlation with TCP concentration. Overall, AKP activity was higher in PVK medium compared to that in NBRIP medium. The highest AKP activity also was observed in PDB medium without added TCP.

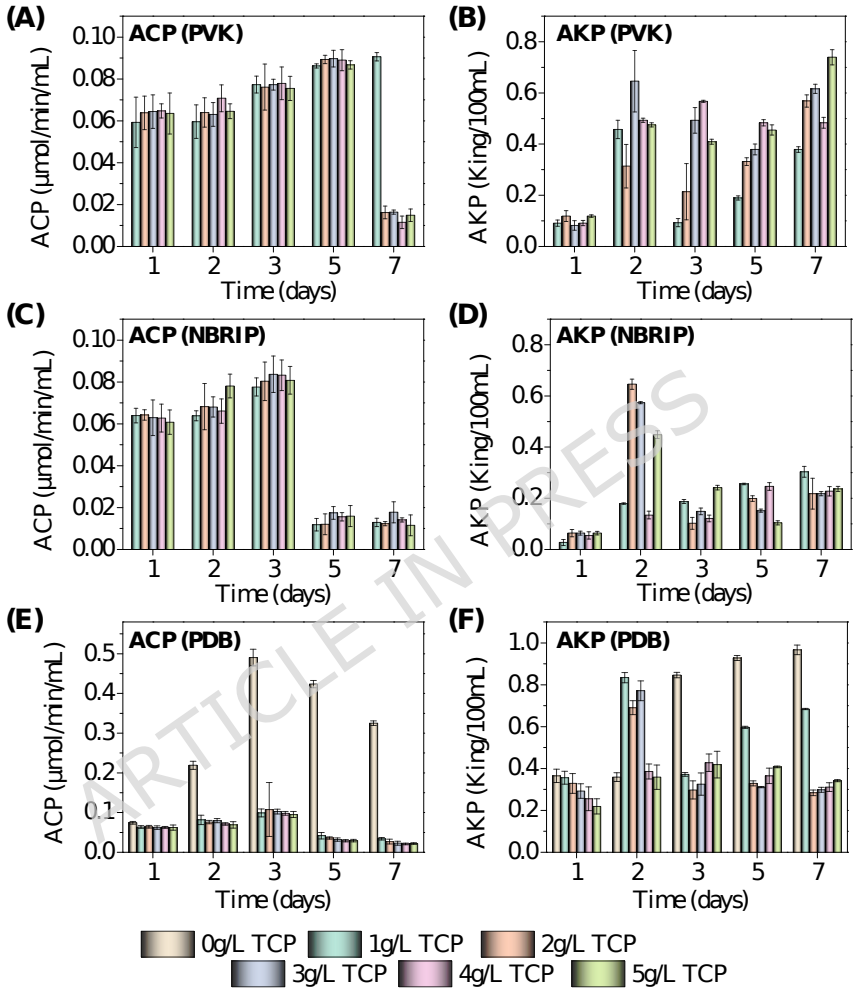

Fig. 4 Changes of ACP and AKP activities along incubation time in PVK medium (A-B), NBRIP medium (C-D) and PDB (E-F) medium, respectively.

Characterization of phosphate-solubilizing products

Fig. 5 shows that no mineral phase formed in PDB medium in the absence of TCP. Whewellite ($CaC_2O_4 \cdot H_2O$) appeared in PVK and PDB medium containing 1g/L TCP. While weddellite ($CaC_2O_4 \cdot 2H_2O$) dominated in other systems. Hydroxyapatite

[$Ca_5(PO_4)_3(OH)$] was detected in PVK and NBRIP media containing 5g/L TCP, which might originate from the conversion of TCP during biological solubilization [20]. Quantitative analysis indicated that weddellite accounted for 72.2% relative abundance in PVK5 and 70.3% relative abundance in NBRIP 5, respectively.

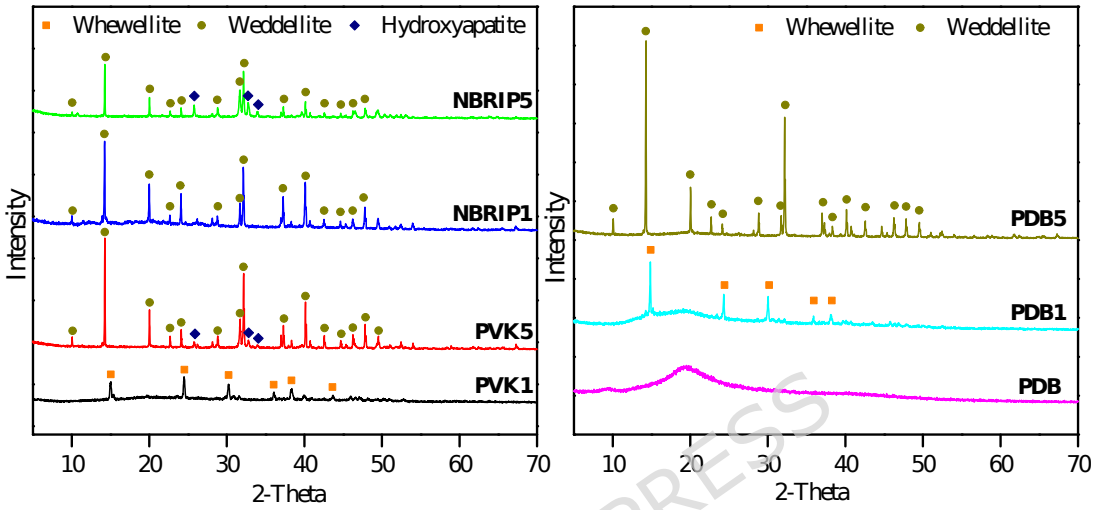

Fig. 5 XRD pattern of sediments in different cultivation systems.

SEM images displaying the micromorphology of hyphae and secondary minerals in different treatments are shown in Fig. 6. Intact hyphae of *Talaromyces* sp. MC-F2 was observed in PDB medium (Fig. S5). Regular-shaped secondary minerals formed in PVK, NBRIP, and PDB media containing TCP, especially when TCP was present at higher concentration. These secondary minerals were similar with the microscopic morphology of calcium oxalate hydrate crystals reported before [21], and aligned with the mineral phase identified by XRD in this study. The result suggested that MC-F2 produced oxalic acid to combine with the released Ca^{2+} to form calcium oxalate.

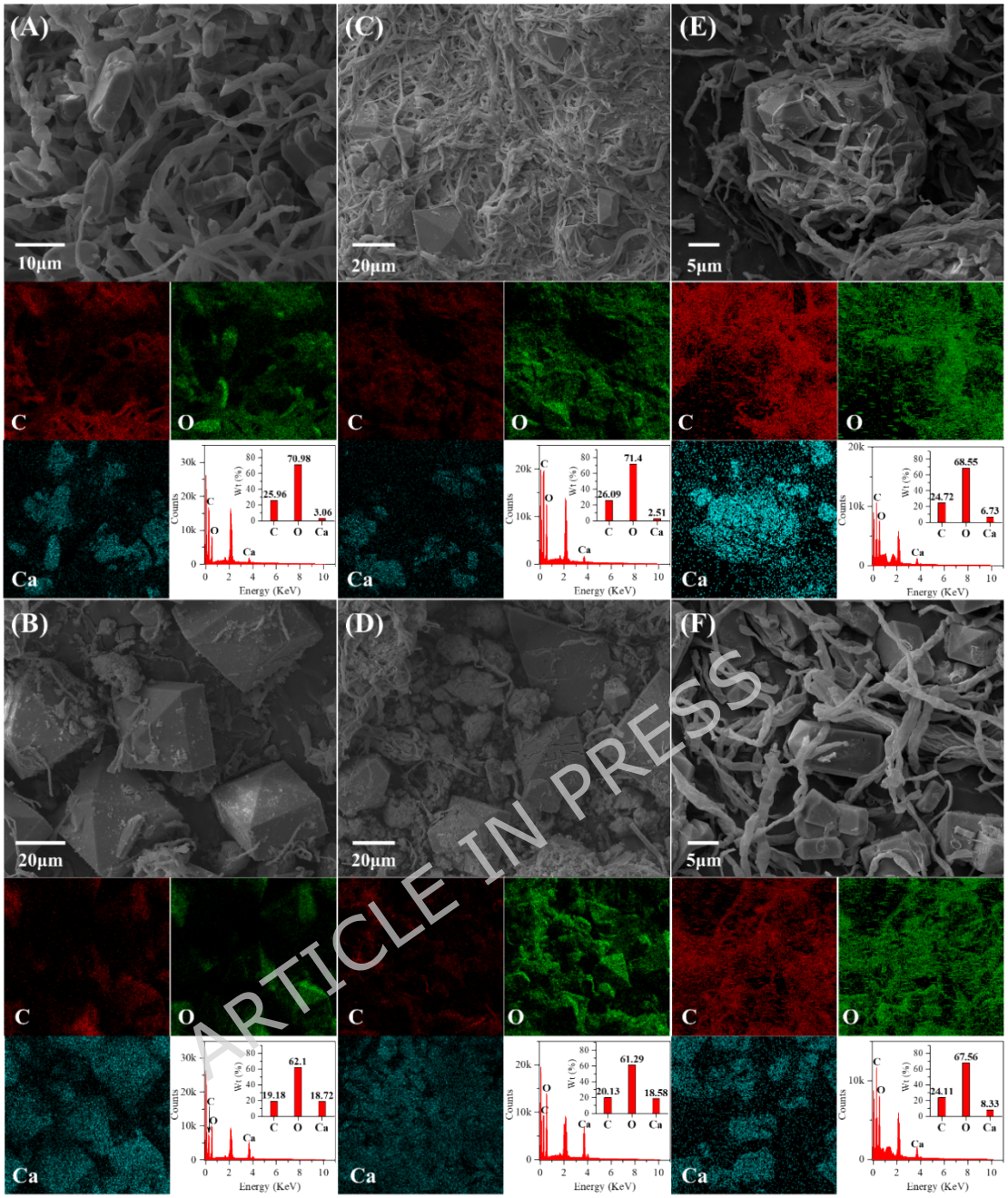

Fig. 6 SEM images of the product in different cultivation systems. (A) PVK1, (B) PVK5, (C) NBRIP1, (D) NBRIP5, (E) PDB1, (F) PDB5.

Fig. S7 illustrates that functional groups on the surface of hyphae were mainly composed of -OH stretching vibration (3415cm^{-1}), C-H stretching vibration (2924cm^{-1}), C=O stretching vibration in amide I and II bands (1656cm^{-1}), -NH or C-H bending vibration (1549cm^{-1}) and -PO_4^{3-} (1035 and 611cm^{-1}) [22]. In media

supplemented with TCP, functional groups exhibited varying degrees of peak shifts or intensity alterations. Specifically, O-H stretching vibration shifted within 3425–3439cm^{-1}. C-H stretching vibration migrated between 2926–2973cm^{-1}. C=O stretching vibration demonstrated significant intensification. -NH or C-H bending vibration showed marked attenuation or even disappearance. The absorption peak of -PO_4^{3-} weakened in PVK medium and NBRIP medium amended with 1g/L TCP.

Source of key components enhancing TCP solubilization

To elucidate the origin of TCP solubilization and calcium oxalate formation, we evaluated and compared phosphate solubilization effects under different experimental modes. As shown in Fig. S8, both two-step and spent medium mode achieved peak soluble P on day 1, which was significantly faster than that in one-step mode. Concurrently, these systems exhibited pronounced pH elevation on day 1, implying substantial consumption of organic acids during TCP solubilization. In contrast, the mycelium system demonstrated weak phosphate-solubilizing capacity, and maintained consistently elevated pH levels. These results collectively indicated that extracellular metabolites secreted by MC-F2 predominantly promoted TCP solubilization.

Furthermore, XRD analysis revealed weddellite was the dominant phase in one-step mode. Two-step mode contained both weddellite and whewellite. Spent medium mode contained whewellite and hydroxyapatite, while mycelium mode exclusively formed hydroxyapatite, with no detectable calcium oxalate crystals. Complementary FTIR spectra (compared against spectra of pure TCP and calcium

oxalate standards, Fig. S6) showed stronger absorption peaks of -OH, -CH_{vs}, C=O and -$CH_{\delta s}$ in mycelium system versus others. The two-step mode exhibited most pronounced spectral alterations, for example, marked attenuation of -OH, -CH_{vs}, -C=O and -PO_4^{3-}, and near-disappearance of -NH/-$CH_{\delta s}$.

Phosphate-solubilizing metabolites analysis by untargeted metabolomics

Both PCA (Fig. S9A) and OPLS-DA (Fig. S9B, C) showed significant differences in tested groups. R^2Y and Q^2 were used to evaluate the modeling and prediction abilities of the OPLS-DA model. The parameters of the OPLS-DA model were all close to 1 (Table S3), suggesting that this model was stable and reliable. The volcano plots suggested significant variations between every two groups (Fig. S9D). A total of 577 (PDB vs PDB1), 415 (PDB1 vs PDB5), 276 (PVK1 vs PVK5) and 240 (NBRIP1 vs NBRIP5) differential metabolites were identified, with 113 (PDB vs PDB1), 281 (PDB1 vs PDB5), 142 (PVK1 vs PVK5), 132 (NBRIP1 vs NBRIP5) metabolites up-regulated expression, and 464 (PDB vs PDB1), 134 (PDB1 vs PDB5), 134 (PVK1 vs PVK5), 108 (NBRIP1 vs NBRIP5) down-regulated expression, respectively (Fig. S10). Focusing on metabolites central to phosphate solubilization, several showed pronounced alterations. Notably, in the comparison where the citrate cycle (TCA cycle) was most active (NBRIP1 vs NBRIP5), citric and malic acid were upregulated by 2.54-fold and 4.87-fold, respectively. Conversely, in the PVK1 vs PVK5 comparison, 2-ketogluconic acid was downregulated by 0.73-fold, aligning with the observed decrease in gluconic acid production at high TCP levels. Gluconic acid was downregulated by 0.59-fold in

the PDB1 vs PDB5 comparison. Key intermediates from other enriched pathways, such as amino acid metabolism, also exhibited significant fold changes, as shown in Table S4-S9.

The classification of differential metabolites is shown in Fig. S11. In the PDB vs PDB1 group, up-regulated metabolites were primarily organoheterocyclic compounds (23.01%), lipids and lipid-like molecules (14.16%), and benzenoids (13.27%). In contrast, down-regulated metabolites largely consisted of organic acids and derivatives (26.29%) and organoheterocyclic compounds (23.49%). For both PDB1 vs PDB5 and PVK1 vs PVK5 groups, organoheterocyclic compounds constituted the majority among up- and down-regulated metabolites. In NBRIP1 vs NBRIP5 group, differential metabolites were mainly categorized as organic acids and derivatives, along with organoheterocyclic compounds.

In Fig. 7, KEGG enrichment pathway analysis suggested that differential metabolites were mainly involved in metabolic pathways. In detail, differential metabolites also enriched in biosynthesis of amino acids, ABC transporters, D-amino acid metabolism, etc. in PDB vs PDB1 group, nucleotide metabolism, ABC transporters, glycine, serine and threonine metabolism, etc. in PDB1 vs PDB5 group, purine metabolism, nucleotide metabolism, arachidonic acid metabolism, etc. in PVK1 vs PVK5 group, ABC transporters, biosynthesis of amino acids and aminoacyl-tRNA biosynthesis, etc. in NBRIP1 vs NBRIP5 group.

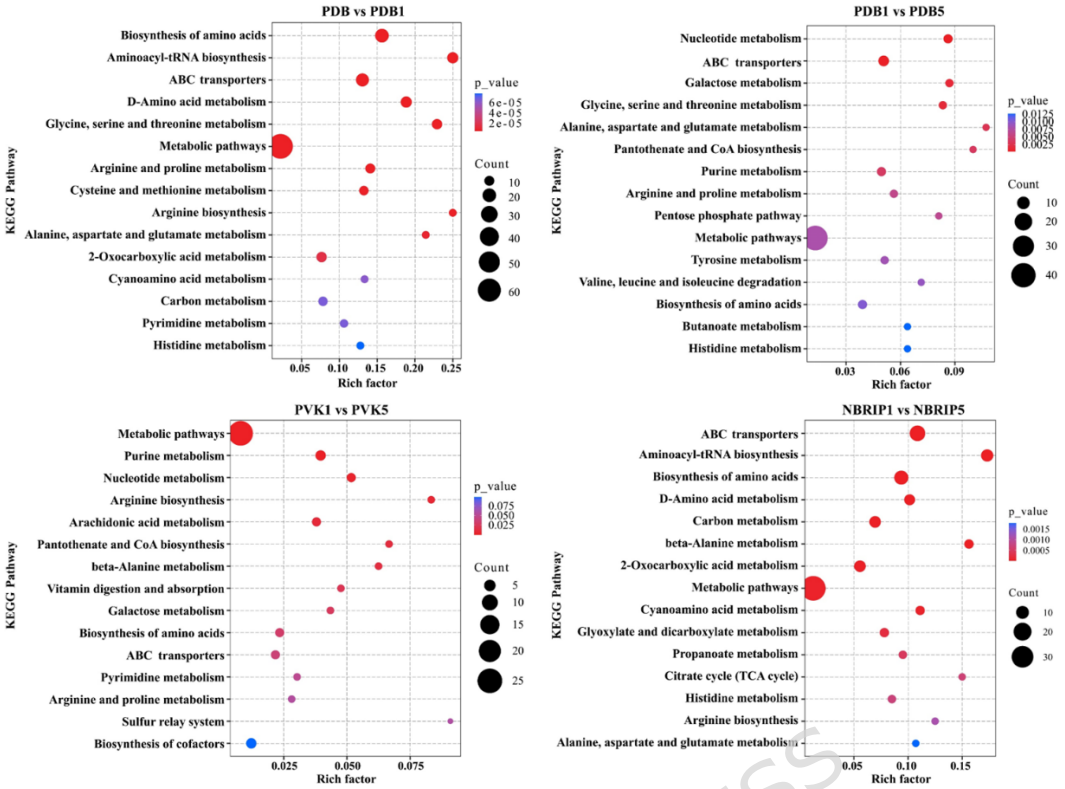

Fig. 7 KEGG enrichment analysis of differential metabolites.

As for KEGG pathway differential abundance score (Fig. S12), all KEGG enrichment pathways were downregulated in the PDB vs PDB1 group, implying the addition of 1g/L TCP inhibited multiple metabolic pathways. In PDB1 vs PDB5 group, only histidine metabolism, galactose metabolism and ABC transporters were downregulated, glycine, serine and threonine metabolism, alanine, aspartate and glutamate metabolism, arginine and proline metabolism were upregulated. It implied that the addition of higher concentration of TCP in PDB medium stimulated the metabolism of some amino acids. In PVK1 vs PVK5 group, galactose metabolism and ABC transporters were downregulated, and arginine biosynthesis, purine and pyrimidine metabolism were upregulated. In NBRIP1 vs NBRIP5 group, arginine biosynthesis, propanoate metabolism and aminoacyl-tRNA biosynthesis were downregulated. TCA cycle was significantly upregulated. Part of key

metabolites involved in organic acids production is displayed in Fig. S13 and Table S4-S9.

Discussion

This study provides one of the first integrated physiological and metabolomic analyses of phosphate solubilization in a *Talaromyces* species. While the secretion of gluconic and malic acids aligns with mechanisms reported in *Aspergillus* and *Penicillium*, our metabolomics data reveal genus- or strain-specific metabolic adaptive strategies.

Talaromyces genus was introduced by Benjamin as a sexual state of *Penicillum,* and it was characterized by soft walled ascomata with interwoven hyphae [23]. In general, *Talaromyces* species have the feature of producing red pigments in the mycelium or diffusing into the agar [24]. MC-F2 possessed typical characteristics of *Talaromyces*, like biverticillate conidiophore, globose ascospores, and abundant diffusing red pigments production. Some *Talaromyces* species have been demonstrated to have phosphate-solubilizing properties, including *T. flavus* [25], *T. pinophilus* [26], *T. funiculosus* [27], *T. nanjingensis* [28], etc. In this study, *Talaromyces* sp. MC-F2 has exhibited effective phosphate solubilization across different media, making it a promising candidate for biofertilizer development.

Usually, NBRIP was regarded more sensitive in comparison to PVK for evaluating phosphate-solubilizing capacity of PSMs [12,29]. For MC-F2, the final concentration of soluble P was highest in NBRIP broth across all tested TCP concentrations. The delayed onset in NBRIP may be attributed to its lower

nitrogen content and absence of complex nutrients like yeast extract (present in PVK), potentially extending the adaptation of MC-F2. Similarly, the rapid initial pH drop and P release in PDB can be attributed to its nutrient-rich medium composition. The early detection of soluble P in PDB even without TCP addition (Fig. 2F) likely originated from the inherent P content of potato extract and/or initial fungal metabolic activity, as the abiotic control ruled out significant chemical dissolution. Phosphate-solubilizing behavior also depends on the specific microbial species. For example, the dissolved P induced by *B. amyloliquefaciens* CZ-B1 in PVK medium was 1.13 times of that in NBRIP medium [30]. Five bacterial species showed phosphate solubilization varying from 535.70 to 618.57μg/mL in NBRIP medium, and 374.20 to 544.28μg/mL in PVK medium with TCP as a source of insoluble phosphate [31]. PDB supplemented with 5g/L TCP was also utilized to cultivate a PSF strain *P. oxalicum*. The maximum soluble P concentration reached 1.05 g/L on day 5 [32], which was lower than that in our results (1.52 g/L in NBRIP with 5 g/L TCP).

Pearson correlation analysis revealed the nuanced regulation of phosphorus solubilization mechanisms by both culture medium and TCP concentration. The strong overall negative correlation in NBRIP reinforces the central role of acidification. In contrast, the condition-specific correlation patterns observed in PDB and PVK indicate that phosphorus solubilization in complex media is a "dynamically decoupled" process. In nutrient-rich PDB under high TCP levels, the strategy may shift from "bulk acidification" to "maintenance of localized

microenvironments." Meanwhile, the negative correlation observed only at a moderate-to-high concentration (4 g/L) in PVK suggests an interaction between its chemical composition (e.g., metal ions, nitrogen source) and TCP concentration, jointly determining the distribution of phosphorus among dissolution, assimilation, and reprecipitation. Therefore, the macroscopic relationship between solution pH and soluble phosphorus is the net outcome of a dynamic balance between underlying microbial physiological activities (acid production, assimilation) and geochemical reactions (dissolution, reprecipitation) under specific environmental conditions, rather than a simple indicator of a single driving force.

PSMs can enhance inorganic phosphate solubilization by releasing low-molecular-weight organic acids [33]. Organic acids production by fungi can be affected by carbon, nitrogen, and phosphate type and concentration [34,35]. The distinct chemical composition of PVK, NBRIP, and PDB media was associated with strikingly different profiles of accumulated organic acids in the culture broth. Gluconic acid and malic acid was the main organic acids appearing in all tested media (Fig. 3). The formation of gluconic acid depends on extracellular direct oxidation of glucose by glucose dehydrogenase [36]. The significantly higher yield of gluconic acid in PDB medium, which contains twice the glucose concentration of PVK and NBRIP, is consistent with the established role of glucose as a direct precursor for extracellular gluconic acid synthesis via glucose dehydrogenase. Previous studies have pointed out that excessive insoluble P can inhibit the growth and metabolism of PSF [37]. The addition of TCP increases the system’s buffering

capacity against fungal acidification, releases Ca^{2+} which can be toxic at elevated concentrations, and alters the ionic milieu. These physicochemical changes undoubtedly contribute to the overall physiological adaptation of MC-F2. It might explain that the productivity of gluconic acid declined when TCP concentration increased in this study. Gluconic acid can be further oxidized to 2-ketogluconic acid by gluconate dehydrogenase [38].

Di- and tricarboxylic acids exhibit higher acidity and stronger chelating capacity than monocarboxylic acids [39]. Malic acid as a kind of dicarboxylic acid is frequently detected in phosphate solubilization. The reported yield of malic acid varied quantitatively among PSMs. The highest amount of malic acid produced by *T. pinophilus* strains ranged from 17.0±1.0 to 250.0±19.6 μg/mL in PVK medium [40]. *Pantoea brenneri* strain 3.2 produced 12.8mM malic acid in NBRIP medium [41] , which was lower than that produced by MC-F2. Compared with the reported *Aspergillus* and *Penicillium* species with phosphate-solubilizing capacity (Table S2), MC-F2 still has advantages in phosphate solubilization and organic acids production. The high secretion of gluconic and malic acids by MC-F2 correlates with its observed phosphate-solubilizing capacity.

It has been widely reported the genus *Aspergillus* and *Penicillum* secreted oxalic acid to accelerate the release of P from Ca-P through the formation of calcium oxalate. Meanwhile, oxalic acid was detectable in the medium [8,21,42,43]. In present work, although XRD (Fig. 5) and SEM (Fig. 6) confirmed the existence of calcium oxalate, oxalic acid was not detected by HPLC in PVK, NBRIP or PDB media. This

implies that oxalic acid secreted by MC-F2 may be produced in low amounts and/or precipitates, preventing its accumulation in the solution above the detection limit. Alternative pathways, such as the direct enzymatic oxidation of glyoxylate or the cleavage of oxaloacetate [44], could also contribute to calcium oxalate formation without substantial free oxalic acid accumulation.

ACP produced by *Aspergillus niger* was under phosphate-mediated repression, that is, high ACP productivity was observed under the condition of low concentration of phosphate [45]. But it was not reflected in our results. Researchers also found that specific ACP was differentially expressed at different culture pH value, with greater production at low pH [46], which is consistent with our results. In general, AKP prevails in alkaline to neutral conditions and has greater affinity to organic phosphorus [4]. The difference of AKP activities may be attributed to relatively higher pH in PVK medium and more organic components in PDB medium compared with NBRIP medium. Additionally, the observed variations in ACP and AKP activities, which did not show a direct statistical correlation with soluble P release, likely reflect a more complex physiological context. These phosphatases are traditionally associated with the mineralization of organic phosphorus compounds [47]. Their elevated activity, particularly in PDB medium without TCP (Fig. 4), may indicate a generalized metabolic state or stress response under phosphate limitation or during active growth, rather than a direct causative role in dissolving inorganic TCP. While MC-F2 possesses substantial phosphatase activity, our data suggest that its remarkable phosphate-solubilizing capacity

against mineral TCP is predominantly mediated by acidification via organic acids, with phosphatase activity representing an associated but not directly rate-limiting physiological trait under these specific conditions.

The source of metabolites participating in phosphate solubilization was clarified by comparing soluble P concentration in one-step, two-step, spent medium, and mycelium modes (Fig. S8). Results indicated that extracellular metabolites mainly contributed to solubilize TCP. Separated mycelium did not favor the formation of calcium oxalate. But in two-step modes, a large number of existing mycelia may promote the formation of calcium oxalate in view of XRD patten and FTIR spectra. Different performances of MC-F2 in one-step, two-step, spent medium and pure mycelia modes illustrated that (1) the co-culture of MC-F2 strain and TCP might inhibited early biological metabolism to some extent, (2) TCP dissolution is the precondition of forming calcium oxalate and mycelium will contribute to crystallization if it did not be separated, possibly through providing nucleation sites or locally modifying microenvironments, (3) the pronounced alterations in functional groups suggest the potential involvement of hyphal surface chemistry in the mineralization process, , which may be more complex than simple chemical precipitation in solution.

The untargeted metabolomics data provide a quantitative metabolic basis for the differential phosphate-solubilizing performance. The marked upregulation of TCA cycle intermediates, particularly the 4.87-fold increase in malate in NBRIP1 vs NBRIP5, provides a direct explanation for the high secretion of malic acid and the

superior solubilization efficiency observed in this medium (Fig. 3, Fig. 2D). This suggests a targeted enhancement of anaplerotic and TCA cycle flux in NBRIP to fuel dicarboxylic acid production. Similarly, the 0.73-fold downregulation of 2-ketogluconate in PVK1 vs PVK5 corresponds quantitatively to the suppressed glucose oxidation pathway and lower gluconic acid yield at high TCP concentration (Fig. 3). These specific, high-magnitude changes in key pathway metabolites underscore that medium composition and TCP load do not merely cause general metabolic shifts but precisely rewire central carbon metabolism in a manner that directly impacts organic acid synthesis and, consequently, phosphate solubilization capacity.

Our work moves beyond confirming the involvement of organic acids to mapping the condition-dependent metabolic network that produces them in a novel fungal agent, thereby identifying key regulatory nodes (e.g., TCA cycle, glucose oxidation) that could be targets for future strain enhancement.

Conclusion

In this study, a novel phosphate-solubilizing fungal strain, *Talaromyces* sp. MC-F2, was successfully isolated and identified. The strain demonstrated efficient TCP solubilization across PVK, NBRIP, and PDB media, with NBRIP medium yielding the highest final soluble P concentrations. The solubilization process was primarily driven by the secretion of organic acids in NBRIP medium, as evidenced by a strong correlation between pH decrease and P release, and led to the formation of calcium oxalate hydrates as secondary minerals. Metabolic analysis further

revealed that medium composition and TCP concentration significantly influenced the expression of key metabolic pathways, particularly those involved in organic acid production. These findings not only expand the resource library of PSF but also enhance our understanding of the metabolic adaptability of PSF under varying environmental conditions. *Talaromyces* sp. MC-F2 shows strong potential for development as an eco-friendly biofertilizer to improve phosphorus availability in agricultural systems. Future studies should focus on field applications, genetic engineering to enhance organic acid synthesis, and the role of specific enzymes such as malate dehydrogenase in regulating acid production. Additionally, integrating transcriptomic and proteomic approaches would help establish causal relationships between metabolic shifts and solubilization phenotypes.

References

1 Lareen, A., Burton, F. & Schafer, P. Plant root-microbe communication in shaping root microbiomes. *Plant Mol. Biol.* **90**, 575-587, doi:10.1007/s11103-015-0417-8 (2016).

2 Santoyo, G. *et al.* Phosphorus-solubilizing microorganisms: Advances in nutrient uptake mechanisms, plant growth promotion, and sustainable agriculture. *Microbiol. Res.* **305**, 128419, doi:https://doi.org/10.1016/j.micres.2025.128419 (2026).

3 Zhu, J., Li, M. & Whelan, M. Phosphorus activators contribute to legacy phosphorus availability in agricultural soils: A review. *Science of the Total Environment* **612**, 522-537, doi:10.1016/j.scitotenv.2017.08.095 (2018).

4 Rawat, P., Das, S., Shankhdhar, D. & Shankhdhar, S. C. Phosphate-solubilizing microorganisms: mechanism and their role in phosphate solubilization and uptake. *J. Soil Sci. Plant Nutr.* **21**, 49-68, doi:10.1007/s42729-020-00342-7 (2021).

5 Li, H. P. *et al.* Roles of phosphate-solubilizing bacteria in mediating soil legacy phosphorus availability. *Microbiol. Res.* **272**, 1-11, doi:10.1016/j.micres.2023.127375 (2023).

6 Nassef, K. *et al.* Phosphate solubilizing microorganisms and their use in sustainable agriculture: a review. *Geomicrobiol. J.* **42**, 224-243, doi:10.1080/01490451.2025.2457660 (2025).

7 Tian, D., Chen, H., Mendes, G. d. O. & Feng, Y. Editorial: Biotechnology of phosphate solubilizing microorganisms for metabolites regulation: present and future. *Front Bioeng Biotech* **11**, 1-2, doi:10.3389/fbioe.2023.1258741 (2023).

8 Tian, D. *et al.* A study of P release from Fe-P and Ca-P via the organic acids secreted by *Aspergillus niger*. *J. Microbiol.* **59**, 819-826, doi:10.1007/s12275-021-1178-5 (2021).

9 Tian, D. *et al.* Lead remediation is promoted by phosphate-solubilizing fungi and apatite *via* the enhanced production of organic acid. *Front Bioeng Biotech* **11**, 1-5, doi:10.3389/fbioe.2023.1180431 (2023).

10 Wang, J. H. *et al.* Metabolomics assisted metabolic network modeling and network wide analysis of metabolites in microbiology. *Crit. Rev. Biotechnol.* **38**, 1106-1120, doi:10.1080/07388551.2018.1462141 (2018).

11 Pikovskaya, R. I. Mobilization of phosphorus in soil connection with the vital activity of some microbial species. *Microbiology* **17**, 362-370 (1948).

12 Nautiyal, C. S. An efficient microbiological growth medium for screening phosphate solubilizing microorganisms. *FEMS Microbiol. Lett.* **170**, 265-270, doi:10.1016/s0378-1097(98)00555-2 (1999).

13 Liao, W., Liu, Y., Frear, C. & Chen, S. A new approach of pellet formation of a filamentous fungus : *Rhizopus oryzae*. *Bioresour. Technol.* **98**, 3415-3423, doi:10.1016/j.biortech.2006.10.028 (2007).

14 Li, Z. *et al.* A study of organic acid production in contrasts between two phosphate solubilizing fungi: *Penicillium oxalicum* and *Aspergillus niger*. *Sci. Rep.* **6**, 1-8, doi:10.1038/srep25313 (2016).

15 Glass, N. L. & Donaldson, G. C. Development of primer sets designed for use with the PCR to amplify conserved genes from filamentous ascomycetes. *Appl. Environ. Microbiol.* **61**, 1323-1330, doi:10.1128/aem.61.4.1323-1330.1995 (1995).

16 Kanehisa, M. & Goto, S. KEGG: kyoto encyclopedia of genes and genomes. *Nucleic Acids Res* **28**, 27-30, doi:10.1093/nar/28.1.27 (2000).

17 Eaton, A. D., Clesceri, L. S., Rice, E. W. & Greenberg, A. E. E. Standard methods for the examination of water and wastewater. *American Public Health Association, Denver, Co* **146–157** (2005).

18 Sarkar, A. *et al.* Screening for phosphate solubilizing bacteria inhabiting the rhizoplane of rice grown in acidic soil in bangladesh. *Acta Microbiol. Immunol. Hung.* **59**, 199-213, doi:10.1556/AMicr.59.2012.2.5 (2012).

19 Gupta, R., Singal, R., Shankar, A., Kuhad, R. C. & Saxena, R. K. A modified plate assay for screening phosphate solubilizing microorganisms. *J. Gen. Appl. Microbiol.* **40**, 255-260 (1994).

20 Xu, K. *et al.* Effects of phosphate-solubilizing bacteria *Aspergillus flavus* AF-LRH1 on promoting phosphorus solubilization, wheat growth and soil heavy metal remediation. *J. Environ. Chem. Eng.* **12**, 1-12, doi:10.1016/j.jece.2024.114357 (2024).

21 Schneider, K. D. *et al.* Comparing phosphorus mobilization strategies using

Aspergillus niger for the mineral dissolution of three phosphate rocks. *J. Appl. Microbiol.* **108**, 366-374, doi:10.1111/j.1365-2672.2009.04489.x (2010).

22 Yue, J. *et al. Penicillium oxalicum* induced phosphate precipitation enhanced cadmium (Cd) immobilization by simultaneously accelerating Cd biosorption and biomineralization. *J. Hazard. Mater.* **470**, 1-11, doi:10.1016/j.jhazmat.2024.134306 (2024).

23 Benjamin, C. Ascocarps of *Aspergillus* and *Penicillium*. *Mycologia* **47**, 669-687 (1955).

24 Yilmaz, N., Visagie, C. M., Houbraken, J., Frisvad, J. C. & Samson, R. A. Polyphasic taxonomy of the genus *Talaromyces*. *Stud. Mycol.*, 175-341, doi:10.1016/j.simyco.2014.08.001 (2014).

25 Della Mónica, I. F. *et al.* Effects of the phosphate-solubilizing fungus *Talaromyces flavus* on the development and efficiency of the Gigaspora rosea-Triticum aestivum symbiosis. *Symbiosis* **64**, 25-32, doi:10.1007/s13199-014-0299-6 (2014).

26 Majumder, M. S. I. *et al.* Comparative study of phosphate solubilization potential of *Talaromyces pinophilus* strains. *Appl. Ecol. Environ. Res.* **17**, 14973-14984, doi:10.15666/aeer/1706_1497314984 (2019).

27 Kanse, O. S., Whitelaw-Weckert, M., Kadam, T. A. & Bhosale, H. J. Phosphate solubilization by stress-tolerant soil fungus *Talaromyces funiculosus* SLS8 isolated from the Neem rhizosphere. *Ann. Microbiol.* **65**, 85-93, doi:10.1007/s13213-014-0839-6 (2015).

28 Sun, X. R. *et al.* Systematic Investigation of Phosphate Decomposition and Soil Fertility Modulation by the Filamentous Fungus *Talaromyces nanjingensis*. *Microorganisms* **13**, 1-20, doi:10.3390/microorganisms13071574 (2025).

29 Alaylar, B., Egamberdieva, D., Gulluce, M., Karadayi, M. & Arora, N. K. Integration of molecular tools in microbial phosphate solubilization research in agriculture perspective. *World J. Microbiol. Biotechnol.* **36**, 1-12, doi:10.1007/s11274-020-02870-x (2020).

30 Zhang, C. *et al.* Isolation and screening of phosphorus solubilizing bacteria from saline alkali soil and their potential for Pb pollution remediation. *Front Bioeng Biotech* **11**, 1-12, doi:10.3389/fbioe.2023.1134310 (2023).

31 Amri, M. *et al.* Isolation, identification, and characterization of phosphate-solubilizing bacteria from Tunisian soils. *Microorganisms* **11**, 14, doi:10.3390/microorganisms11030783 (2023).

32 Hao, S. *et al.* Combined effects of *Penicillium oxalicum* and tricalcium phosphate on lead immobilization: Performance, mechanisms and stabilities. *Ecotoxicol. Environ. Saf.* **227**, 1-9, doi:10.1016/j.ecoenv.2021.112880 (2021).

33 da Silva, L. I. *et al.* Phosphorus-solubilizing microorganisms: a key to sustainable agriculture. *Agriculture-Basel* **13**, doi:10.3390/agriculture13020462 (2023).

34 Vassilev, N., Mendes, G., Costa, M. & Vassileva, M. Biotechnological tools for enhancing microbial solubilization of insoluble inorganic phosphates.

Geomicrobiol. J. **31**, 751-763, doi:10.1080/01490451.2013.822615 (2014).

35 Stefanoni Rubio, P. J. *et al.* Carbon and nitrogen sources influence tricalcium phosphate solubilization and extracellular phosphatase activity by *Talaromyces flavus*. *Curr. Microbiol.* **72**, 41-47, doi:10.1007/s00284-015-0914-7 (2016).

36 Goldstein & Alan, H. Recent Progress in Understanding the Molecular Genetics and Biochemistry of Calcium Phosphate Solubilization by Gram Negative Bacteria. *Biol Agric Hortic* **12**, 185-193 (1995).

37 Fenice, M., Selbman, L., Federici, F. & Vassilev, N. Application of encapsulated *Penicillium variabile* P16 in solubilization of rock phosphate. *Bioresour. Technol.* **73**, 157-162, doi:10.1016/s0960-8524(99)00150-9 (2000).

38 Kataoka, N. Ketogluconate production by Gluconobacter strains: enzymes and biotechnological applications. *Biosci., Biotechnol., Biochem.* **88**, 499-508, doi:10.1093/bbb/zbae013 (2024).

39 Ma, Y. *et al.* Phosphate solubilizing fungi enhance insoluble phosphate dissolution via organic acid production: mechanisms and applications. *Front. Microbiol.* **16**, 1-6, doi:10.3389/fmicb.2025.1600231 (2025).

40 Majumder, M. *et al.* Organic acid production efficiency of different phosphate solubilizing *Talaromyces pinophilus* strains. *Appl. Ecol. Environ. Res.* **23**, 97-108, doi:10.15666/aeer/2301_097108 (2025).

41 Suleimanova, A. *et al.* Phosphate Solubilization and Plant Growth Promotion by *Pantoea brenneri* Soil Isolates. *Microorganisms* **11**, 1-18, doi:10.3390/microorganisms11051136 (2023).

42 Mendes, G. d. O. *et al.* Mechanisms of phosphate solubilization by fungal isolates when exposed to different P sources. *Ann. Microbiol.* **64**, 239-249, doi:10.1007/s13213-013-0656-3 (2014).

43 Mendes, G. d. O. *et al.* Chemical and physical mechanisms of fungal bioweathering of rock phosphate. *Geomicrobiol. J.* **38**, 384-394, doi:10.1080/01490451.2020.1863525 (2021).

44 Gadd, G. M. Fungal production of citric and oxalic acid: importance in metal speciation, physiology and biogeochemical processes. *Adv. Microb. Physiol.* **41**, 47-92, doi:10.1016/s0065-2911(08)60165-4 (1999).

45 MacRae, W. D. *et al.* A phosphate-repressible acid phosphatase gene from *Aspergillus niger*: its cloning, sequencing and transcriptional analysis. *Gene* **71**, 339-348, doi:10.1016/0378-1119(88)90051-0 (1988).

46 Hidayat, B. J., Eriksen, N. T. & Wiebe, M. G. Acid phosphatase production by *Aspergillus niger* N402A in continuous flow culture. *FEMS Microbiol. Lett.* **254**, 324-331, doi:10.1111/j.1574-6968.2005.00045.x (2006).

47 Della Monica, I. F., Godoy, M. S., Godeas, A. M. & Scervino, J. M. Fungal extracellular phosphatases: their role in P cycling under different pH and P sources availability. *J. Appl. Microbiol.* **124**, 155-165, doi:10.1111/jam.13620 (2018).

Statements and Declarations

Funding This work was supported by the Fundamental Research Funds for the Central Universities (Grand NO. 2024QN11034).

Competing interests The authors declare no competing interests

Author Contributions Mingchen Xia: Writing – original draft, Conceptualization, Visualization, Investigation, Formal analysis, Data curation, Funding acquisition. Peng Bao: Investigation, Methodology, Formal analysis, Data curation. Shilong He: Writing – review & editing. Guanzhou Qiu: Writing – review & editing. Weimin Zeng: Writing – review & editing. Yu He: Investigation.

Data Availability The ITS rRNA gene sequence of *Talaromyces* sp. MC-F2 is available in GenBank under Accession Number PP358163, accessible at https://www.ncbi.nlm.nih.gov/nuccore/PQ270042.1/

Figure legends

Fig. 1 Transparent halo observation (A), SEM image (B) and phylogenetic tree based on ITS gene sequence (C) of the isolated PSF strain

Fig. 2 Changes of pH and soluble P concentration along incubation time in PVK medium (A-B), NBRIP medium (C-D) and PDB (E-F) medium.

Fig. 3 Types and quantities of produced organic acids by MC-F2 in PVK, NBRIP and PDB liquid medium with 1g/L or 5g/L TCP. Data are shown as final supernatant concentration (mean ± SD, n=3).

Fig. 4 Changes of ACP and AKP activities along incubation time in PVK medium (A-B), NBRIP medium (C-D) and PDB (E-F) medium, respectively.

Fig. 5 XRD pattern of sediments in different cultivation systems.

Fig. 6 SEM images of the product in different cultivation systems. (A) PVK1, (B) PVK5, (C) NBRIP1, (D) NBRIP5, (E) PDB1, (F) PDB5.

Fig. 7 KEGG enrichment analysis of differential metabolites.